Lumped thermal analysis of traction motors for effective thermal management with Machine Learning approach

G. Amba Prasad Rao[1], Ganesh Madhusudhanan P[2]
[1]*Corresponding Author, Professor, Department of Mechanical Engineering, National Institute of Technology Warangal-506 004, Telangana, India*
ORCID: https://orcid.org/0000-0003-1764-3478
[2]*Department of Mechanical Engineering National Institute of Technology Warangal-506 004, Telangana, India*

***Abstract*—The market share of electric vehicles is increasing due to the persistent issues of high harmful emissions due to the combustion of fossil liquid fuels for use in conventional prime movers. Electric motors and batteries are important components of a typical neat electric vehicle. Electric motors, especially Permanent Magnet Motors, are crucial in electric vehicles due to their superior torque-to-inertia ratio, power density, and efficiency. This study explores thermal analysis techniques for Permanent Magnet Synchronous Motors to determine temperature variations and identify areas requiring effective thermal management. Using a lumped thermal network and linear equations in MATLAB, the analysis captures both axial and radial heat transfer in the motor. Temperatures obtained from the lumped model for the winding, rotor, stator, permanent magnet, and casing are 123.76°C, 114.87°C, 120.91°C, 114.87°C, and 87.49°C, respectively. The obtained temperatures align well with Computational Fluid Dynamics (CFD) results and experimental data, highlighting the highest winding temperature during continuous operation at 4500 rpm. The thermal network aids in material selection, insulation, cooling methods, and component design. Additionally, various machine learning algorithms, including Linear Regression, Decision Tree, Random Forest, and Support Vector Machines, predict temperature distributions across different motor geometries. The Linear Regression model yielded the highest R-squared value, closely aligning with the lumped model's predictions for the winding, rotor, casing, permanent magnet, and stator temperatures.**

***Index Terms*—Electric Vehicle; Thermal network; Lumped Parameter; Permanent Magnet Synchronous Motor; Machine Learning.**

Abbreviations

CFD	Computational Fluid Dynamics
IPSM	Interior Permanent Magnet Synchronous motors
LH	Lumped Heat transfer
LP	Lumped Parameter
MAE	Mean Absolute Error
PMSM	Permanent Magnet Synchronous motors
RMSE	Support Vector Regression
RTD	Resistance Temperature Detector
SVR	Support Vector Regression

1. INTRODUCTION

High-performance electric motors required for traction applications necessitate high torque and power densities. The increased current densities associated with these demands lead to elevated heating of the stator winding and higher copper losses. Effective heat dissipation from the winding to the motor casing and the external environment is essential for maintaining optimal motor performance [1, 2]. Heat dissipation techniques typically involve the use of cooling fins and, in some cases, enclosed fans. However, for applications with substantial torque demands, forced cooling methods such as liquid cooling are required to manage the significant heat generated by the winding [3]. Commonly used cooling liquids include water and oil [4]. Liquid cooling is particularly beneficial in high-torque scenarios as it maintains consistent temperature control of both the stator and rotor while potentially reducing the overall motor size.

To optimize motor design and identify critical locations susceptible to high temperatures, precise investigation of temperature distribution across various motor regions is essential. Lumped parameter modeling is commonly employed for this purpose and is frequently used alongside numerical approaches. While Computational Fluid Dynamics (CFD) can be time-consuming, it provides accurate results; therefore, techniques such as Lumped Heat Transfer (LH) analysis are preferred for quicker and approximate temperature distributions [5, 6]. LH analysis assists in identifying problematic regions and optimizing motor geometry [7, 8]. Research has applied LH analysis to different motor types, including Interior Permanent Magnet Motors (IPSM) in both air-cooled and liquid-cooled configurations [9-12], and has examined temperature variations across various water jacket designs [13]. To address complex liquid cooling arrangements, integrative methodologies combining CFD and LH analysis have been proposed [14, 15]. Synchronous motors have also benefited from LH analysis, leading to improved designs based on temperature data [16, 17]. Additionally, research has investigated various fan shapes for enclosed fans in electric motors to enhance heat transfer and efficiency [18, 19]. A comprehensive thermal analysis of electric motors requires an understanding of complex thermal phenomena beyond basic geometrical and material properties. Integrating CFD with empirical data enhances model precision, and experimental calibration further refines predictive accuracy [20].

The current trend in railway development focuses on optimizing energy usage, especially during braking phases. Researchers have developed a new modeling approach using Matlab-Simscape™ to analyze energy optimization in railway systems. The model was validated on an Italian High-speed line and train, showing potential for energy savings with the use of energy storage devices [21].
An Advanced Dynamic Model Predictive Control (AMPC) based on a Nonlinear Model Predictive Control (NMPC) framework with a multi-objective cost function is proposed to improve the energy performance of fuel cell hybrid electric vehicles while prolonging their component lifetime. Dynamic weights are used to formulate the cost function as a combination of fuel consumption, rate of change of fuel cell power, battery power, fuel cell efficiency, state of charge of the battery, and their temperatures. A fuzzy cognitive map (FCM) is designed to regulate the dynamic weights online and adjust the importance of each cost component according to driving conditions. The efficacy of the proposed AMPC is illustrated through simulation using a FCHEV model from the simulation tool ADVISOR [22].

A work on the impact of thermal management on the driving range of electric vehicles, specifically the Tesla Model S and Model 3. The study includes a parametric analysis of various factors, such as air conditioning usage, vehicle size, driving cycle, and ambient temperature, on the range of the vehicles. The results indicate that turning on the air conditioning system could potentially reduce the electric vehicle range by 38–45% in city driving conditions. Additionally, higher ambient temperatures significantly decrease the range, with a 13.4% decrease for the Tesla Model 3 when the temperature rises from 35°C to 40°C. The study's code is available as open source on GitHub for further analysis and concept design of electric vehicle thermal management [23].

A thermal equivalent circuit (TEC) was used to analyze the temperature of a wound rotor synchronous motor (WRSM) with a water-cooling jacket. The TEC analysis results matched well with experimental and numerical data, demonstrating its effectiveness in estimating WRSM temperatures [24].

The technical feasibility and potential of an air-cooled traction inverter for mid-sized passenger vehicles has been investigated , with very high heat fluxes and heat loads. The system uses a heat pipe based air-cooled heat sink for thermal management of the inverter. The proposed solution was able to keep the junction temperature within the required limits, provide thermal uniformity, handle maximum power surges, and qualify for start-up from a frozen state. This air cooling system provides a dedicated and modular approach, with operational safety, runtime reliability, and lower system cost compared to liquid-cooled systems, making it critical for automotive applications [25].

An overview of integrated motor drives (IMDs) with a focus on thermal management of high-specific-output and high-efficiency electrical machines. It discusses the evolution of IMDs from the 1960s to the present, highlighting the integration of electronics with electrical machines and the challenges associated with effective heat removal from the machine composite structure. The review also explores the use of advanced motor cooling techniques such as direct winding oil spray cooling, forced air rotor cooling, and indirect stator-winding heat exchanger cooling. Additionally, it mentions the use of additive manufacturing, highly integrated heat exchangers, multi-functional composite materials, and phase change heat transport and heat storage as promising solutions for the next generation of IMDs [26].

A parameter-based and thermal model for estimating rotor temperature in induction machines has been developed, demonstrating effectiveness under both full and low load conditions, with estimated temperatures within 5°C, 10°C, and 2°C of measured values for 1.5 kW, 18.5 kW, and 210 kW machines, respectively. Discrepancies arise from measurements being taken at the end ring rather than directly from the rotor [27]. The thermal network model accurately predicts temperatures for a squirrel cage induction motor at rated load, with errors generally remaining within practical limits [28]. For a Totally Enclosed Fan-Cooled (TEFC) induction machine, simulations using CFD and a Thermal Equilibrium Model (TEC) are compared with data from Infrared Camera (IR) sensors, Infrared Sensors (IRS), and IR thermal cameras. The CFD model accurately predicts steady-state temperatures, while the TEC model, incorporating thermal capacitances and transient cycles, shows a maximum deviation of 10°C from measurements for both continuous and intermittent loading cases, indicating satisfactory accuracy [29].

Recent advancements underscore the growing significance of machine learning (ML) in electric vehicle (EV) technology, leading to innovations in motor design, performance optimization, and predictive maintenance. Machine learning models, especially neural network (NN) estimators, have shown strong performance in predicting motor position and speed across various dynamic profiles, with minimal impact from inductance matrix saturation, making them suitable for sensorless drives in electric vehicles [30]. Additionally, a multi-objective optimization procedure utilizing an advanced model and machine learning has identified several design candidates, with one selected for its optimal performance characteristics. Experimental validation confirmed significant improvements in key metrics, and the optimization process effectively reduced computational time, demonstrating its feasibility for large-scale applications [31]. Furthermore, machine learning results indicate that the Fine Tree method excels in forecasting the speed and torque of permanent magnet synchronous motors, proving effective for electric vehicle design with minimal Root Mean Square Error (RMSE). Nonetheless, challenges persist regarding the model's robustness across different Original Equipment Manufacturers (OEMs) and varying parameters, as well as its handling of motor aging, presenting opportunities for further research [32].

The present study is distinguished by its use of a lumped model to capture the motor's transient behavior. Unlike conventional models that focus primarily on steady-state conditions, this study incorporates dynamic aspects to provide a more comprehensive understanding of motor operation. Additionally, the motor's winding structure is distributive, which contrasts with the predominantly concentrated windings used in other models. The model's validity is further reinforced through experimental validation under real-world operating conditions. The inclusion of transient behavior and real-world validation enhances the model's reliability and applicability, offering valuable insights for both theoretical analysis and practical engineering applications. Furthermore, machine learning models are employed to estimate the temperature of motor components, facilitating an understanding of temperature variations within the motor across different geometries.

The methodology for designing and implementing the lumped parameter model and the setup for the Computational Fluid Dynamics (CFD) analysis is presented in detail. It includes the assumptions made, the calculation of thermal resistances and capacitances, and the boundary conditions applied. Further, the experimental setup and machine learning

models used for temperature prediction will also be elaborated. The results obtained from the lumped parameter model and the CFD analysis will be compared and analyzed. The performance of different machine learning models in predicting temperature profiles will also be discussed, highlighting their accuracy and applicability in the thermal management of traction motors.

II. METHODOLOGY

A. Lumped Parameter Modelling

Elevated temperatures within the slots can cause the slot insulation to deteriorate, reducing the lifespan of both the motor and its insulation. Hence, there is a necessity for accurate prediction of the temperature in the motor. An electric motor has many complex geometries; hence, to model them, a large thermal model with all paths is required. However, with an increase in the paths, the complexity and time required for calculation will also increase due to the complex geometry and large calculations required. To address this challenge, it is essential to develop a simple, efficient, and compact model that can accurately predict the motor's critical temperature. Therefore, the symmetry of the motor is invoked, and certain assumptions like losses are distributed uniformly in the machines; the axial heat transfer on the shaft and windings is focused; and the temperature of the casing is uniformly distributed. The use of these assumptions and symmetry reduces the number of nodes and pathways.

The conduction resistance can be evaluated using the hollow cylinder formula, thus reducing the complexity of the thermal model.

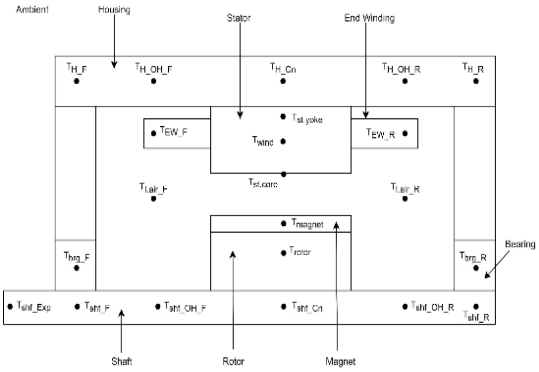

Fig. 1: Detailed Illustration of Motor's Physical Structure showing key components and their spatial arrangement

Table 1: Detailed Specifications of Thermal Nodes

Symbol	Description	Symbol	Description
amb	Ambient	I.air	Inside Air
Brg	Bearing	OH	Over Hang
Cn	Center	R	Rear
EW	End Winding	Rot	Rotor
Exp	Exposed	shf	Shaft
F	Front	st	Stator
H	Housing	W	Winding

The steady LP formulation for the PMSM motor described is depicted in Fig. 2. This formulation comprises 22 nodes, symbolizing crucial thermal elements and temperature elevations. Since the slots primarily contribute to heat production and the end windings endure the highest temperature in the motor, the design procedure and LP formulation give importance to the windings. As a result, more nodes are integrated to precisely assess the winding temperature. Radial modeling is used for these elements, and homogeneous axial temperature variation is assumed. There's no gradient in temperature in the geometry. The housing part enclosing the stator, the rotor, the magnet, and the shaft beneath the rotor cover are all modeled as cylinders. Radial heat transfer is considered in the stator, air gap, rotor, magnet, and active windings. In contrast, the shaft, end winding, and housing cases account for both axial and radial heat transfers. Convection resistances between the inner air and the shaft's front and rear sections, end winding, and bearing are taken into account. Both convection and radiation modes account for heat transfer from the housing to the surrounding air. However, radiation from internal surfaces is neglected. Losses are allocated to their corresponding components, and based on the volume of active winding, front-end winding, and rear-end winding, copper losses are

Table 2: Breakdown of Power Losses in Motor Components

Symbol	Description
P_{Brg}	Power loss from Bearing
P_{EW_F}	Power loss from Front End Winding
P_{EW_R}	Power loss from rear-end winding
P_{Magnet}	Power loss from Magnet
P_{Rotor}	Power loss from Rotor
P_{Stator}	Power loss from Stator
P_W	Power loss from Winding

Table 3: Specifications of Capacitors in Motor System

Symbol	Description
C_{Brg}	Bearing Capacitance
C_{EW_F}	Front End Winding Capacitance
C_{EW_R}	Rear End Winding Capacitance
C_H	Housing Capacitance
C_{Magnet}	Magnet Capacitance
C_{Rotor}	Rotor Capacitance
C_{shf}	Shaft Capacitance
C_{Stator}	Stator Capacitance
C_W	Winding Capacitance

distributed accordingly. In the construction of a lumped model for thermal analysis, thermal resistances are incorporated to account for changes in material properties and multiple modes of heat transfer. When there is a transition from one material to another, such as from the rotor to the shaft, a thermal resistance is introduced to represent the change in thermal conductivity and material characteristics. Similarly, when more than one mode of heat transfer is involved, such as conduction from the stator to the enclosure and convection from the enclosure to the atmosphere, additional resistances are added to the model. This approach ensures that the lumped model accurately reflects the complexity of heat transfer processes within the motor. By systematically analyzing the changes in materials and the interactions of various heat transfer mechanisms, a comprehensive and precise lumped thermal model can be developed, enhancing the prediction of temperature profiles across different motor components under various operating conditions.

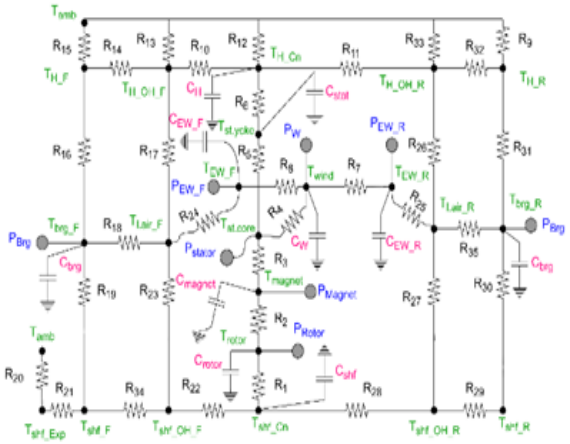

Fig. 2: Electrical Resistance Model Applied to Motor Components.

Table 4: Resistance for Various Motor Components

Resistance No.	Description
R1	Conduction from Rotor to Stator
R2	Conduction from Magnet to Rotor
R3	Convection from Stator to Magnet (Air Gap)
R4	Conduction from Windings to Stator core
R5	Conduction from Stator core to Stator yoke
R6	Conduction from Stator yoke to Housing
R7	Conduction from Winding to Rear End winding
R8	Conduction from Winding to Front End winding
R9	Convection from Rear Housing to ambient
R10	Conduction from Housing Center to Front Overhang Housing
R11	Conduction from Housing Center to Rear Overhang Housing
R12	Convection from Housing centre to ambient
R13	Convection from Front Overhang Housing to ambient
R14	Conduction from Front Overhang Housing to Front Housing
R15	Convection from Front Housing to ambient
R16	Conduction from Front bearing to Front Housing
R17	Convection from Front Inside air to Front Overhang Housing
R18	Convection from Front Bearing to Front Inside Air

Resistance No.	Description
R19	Conduction from Front Shaft to Front Bearing
R20	Convection from Exposed Shaft to ambient
R21	Conduction from Front Shaft to Exposed Shaft
R22	Conduction from Shaft Center to Front Overhang Shaft
R23	Convection from Front Overhang Shaft to Front Inside Air
R24	Convection from Front End Winding to Front Inside Air
R25	Convection from Rear End Winding to Rear Inside Air
R26	Convection from Rear Inside air to Rear Overhang Housing
R27	Convection from Rear Overhang Shaft to Rear Inside Air
R28	Conduction from Shaft Center to Rear Overhang Shaft
R29	Conduction from Rear Overhang Shaft to Rear Shaft
R30	Conduction from Rear Shaft to Rear Bearing
R31	Conduction from Rear bearing to Rear Housing
R32	Conduction from Rear Overhang Housing to Rear Housing
R33	Convection from Rear Overhang Housing to ambient
R34	Conduction from Front Overhang Shaft to Front Shaft
R35	Convection from Front Bearing to Rear Inside Air

B Resistance calculation

Rotor shaft conduction resistance

The rotor and shaft are made up of cylindrical components so, the resistance between the rotor and shaft.

$$R = \frac{\ln\left(r_{\text{rotor}} / r_{\text{shaft}}\right)}{2\pi k_{\text{rotor}} L} \tag{1}$$

Where, r_{rotor} is the rotor radius, r_{shaft} denotes shaft radius, k_{rotor} represents the rotor's thermal conductivity and L denotes rotor axial length.

Rotor magnet conduction resistance

Similarly, the magnets are placed on top of the rotor and hence the resistance between the rotor and the magnet can be calculated with an equivalent cylinder with $n\theta$ radian. The resistance between the rotor and magnet is as follows

$$R = \frac{\ln\left(r_{\text{magnet}} / r_{\text{rotor}}\right)}{n\theta k_{\text{m}} L} \tag{2}$$

Where, r_{magnet} is the radius of the magnet, n denotes the pole numbers, θ represents one pole in radian and k_{m} represents the magnet's thermal conductivity.

Air gap convection resistance

The convection resistance in the air gap between the stator and the rotor is evaluated using the Taylor-Coutte flow. The Taylor-Couette flow describes the fluid dynamics in the air gap without axial flow. The air gap's hydraulic diameter (D_h), which can be explained by the geometry of a concentric annulus, must be chosen to calculate the Reynolds number [28]:

$$D_h = \frac{4 \cdot A}{P} = \frac{4 \cdot \frac{\pi \cdot \left(D_{S,i}^2 - D_{R,o}^2\right)}{4}}{\pi \cdot \left(D_{S,i} - D_{R,o}\right)} = D_{S,i} - D_{R,o} \tag{3}$$

Where, $D_{S,i}$ is the inner diameter of the stator and $D_{R,o}$ is the outer diameter of the Rotor

Further, Reynolds number for air gap is provided by:

$$Re_{A.gap} = \frac{\omega_R \cdot R_{R,o} \cdot D_h}{v_A} = \frac{\omega_R \cdot R_{R,o} \cdot 2 \cdot w_{A.gap}}{v_A} \tag{4}$$

Where, ω_R denotes the rotor angular velocity and v_A denotes air kinematic viscosity.

Taylor's number for air gap is described as:

$$Ta_m = Re_{A.gap}^2 \cdot \frac{w_{A.gap}}{R_{o,R}} = \frac{\omega_R^2 \cdot R_{R,o} \cdot \left(\frac{D_h}{2}\right)^3}{v_A^2} \tag{5}$$

Further using the Taylor number, the Nusslet number (Nu) is determined using the heat transfer coefficient ($h_{A.gap}$) between the air gap and the stator is evaluated.

$$Nu_{A.gap} = \begin{cases} 2 & Ta_m < 1700 \\ 0.128 \cdot Ta_m^{0207} & 1700 < Ta_m < 10^4 \\ 0.409 \cdot Ta_m^{0241} & 10^4 < Ta_m < 10^7 \end{cases} \tag{6}$$

$$Nu_{A.gap} = \frac{h_{A.gap} \cdot D_h}{k_A} \tag{7}$$

Where, k_A is the thermal conductivity of air.

Resistance in the air gap between the stator and rotor is as follows

$$R = 1 / A_{\text{A.gap}} \cdot h_{\text{A.gap}} \tag{8}$$

Stator teeth conduction resistance

The stator is divided into two sections: the stator teeth and the stator yoke, to calculate the resistance of the stator accurately. The teeth are modeled with the percentage factor.

$$R = \frac{\ln\left(r_{sm} / r_{si}\right)}{2\pi k_s L_s p} \tag{9}$$

Where, r_{si} denotes stator inner radius, r_{sm} denotes stator means yoke radius, k_s denotes stator thermal conductivity and p denotes the teeth section percentage to all of the teeth with the slots.

Stator yoke resistance

Stator yoke resistance is calculated using the mean radius of the stator yoke (r_{sm}) and outer stator yoke radius (r_{so}).

$$R = \frac{\ln\left(r_{so} / r_{sm}\right)}{2\pi k_s L_s} \tag{10}$$

Where, k_s denotes stator thermal conductivity and L_s denotes the stator axial length.

End winding convection resistance

To determine the convection resistance of the end winding the convection coefficient is evaluated using the Schubert's model [29].

$$h_{ew} = 15.5 \times \left\{1 + \left(0.4 v_{\text{i.air}}\right) 0.9\right\} \tag{11}$$

$$v_{\text{i.air}} = r_{\text{rot}}\, \omega \eta \tag{12}$$

$$R = 1 / A_{\text{ew}} \cdot h_{\text{ew}} \tag{13}$$

Where, h_{ew} denotes the combination of forced and free convection coefficient of end winding, η is the rotor efficiency and A_{ew} is the end winding area.

Casing resistance

Heat transfer in the casing is caused by both radiation and convection. So, to determine the casing both convection and radiation resistance are calculated and summed up together.

Radiation from the casing is calculated by

$$R = \frac{1}{\sigma \varepsilon A_{rad} \left\{\left(T_{amb} + T_{\text{fin}}\right) \times \left(T_{amb}^2 + T_{\text{fin}}^2\right)\right\}} \tag{14}$$

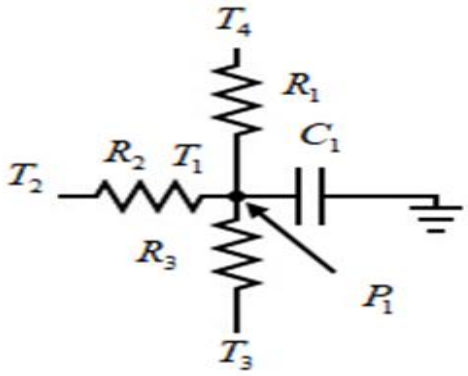

Fig. 3: Schematic of Simplified Thermal Resistance Network

Where, σ denotes Stefan-Boltzmann constant, ε represents emissivity, A_{rad} represents the radiation surface area and T_{fin} is the fin temperature.

$$R = \frac{1}{A_{fr} \cdot h_{fin}} \tag{15}$$

Where, A_{fr} denotes the fin area and h_{fin} denotes the forced convection coefficient of the fin. It can be calculated as follows.

$$h_{fin} = \left(\rho c_p D v_{fin}\right) / \left[4 \times L_{fin} \times \left(1 - e^{-m}\right)\right] \tag{16}$$

$$m = \frac{0.1448 L_{\text{fin}}^{0.946}}{D^{1.16} \times \left\{\kappa_{\text{fin}} / \rho c_{\text{p}} v_{\text{fin}}\right\}^{0.214}} \tag{17}$$

Where D denotes the fin hydraulic diameter, L denotes the fin length and v is the air velocity across the fin.

The final resistance can be determined by adding the convection and conduction resistance.

Other resistances can be easily calculated using the corresponding axial length and the cross-sectional area. To determine the transient response of the system capacitance is added to the resistance model. The capacitance is evaluated by multiplying the mass of the component in *kg* with the specific heat capacity of the component in $J / kg \cdot K$.

C Node Equation

The representation of a particular element using nodes, along with its associated thermal resistances to the environment, is referred to as a node configuration. The node layout shown below is used to calculate temperature T1 from Fig.3.

$$\left(\frac{T_1-T_2}{R_2}\right)+\left(\frac{T_1-T_3}{R_3}\right)+\left(\frac{T_1-T_4}{R_1}\right) \quad (18)$$

$$\left(\frac{1}{R_2}+\frac{1}{R_1}+\frac{1}{R_3}\right)T_1-\left(\frac{1}{R_2}\right)T_2-\left(\frac{1}{R_3}\right)T_3-\left(\frac{1}{R_1}\right)T_4+C_1\frac{dT_1}{dt}=P_1 \quad (19)$$

Where R is the resistance, T is the temperature, C is the capacitance and P is power loss.
Further Equation (19) is written in matrix form as.

$$C\frac{dT}{dt}=P-GT \quad (20)$$

Where C denotes the capacitance matrix, P is the power loss matrix and T is the temperature matrix.

D CFD analysis

Only the elements deemed necessary from a fluid-dynamic perspective are addressed to achieve this goal. For instance, the study does not include washers, tie rods, O-rings, or any other items crucial to the mechanical seal and assembly. This is done not just to obtain a simplified version but also to reduce the model's size and, in turn, the amount of mesh cells generated, so simplifying and speeding up the calculation process. It is a well-known fact that adding a significant number of details that are in excess from a thermal perspective can make meshing more difficult and increase the likelihood of errors.

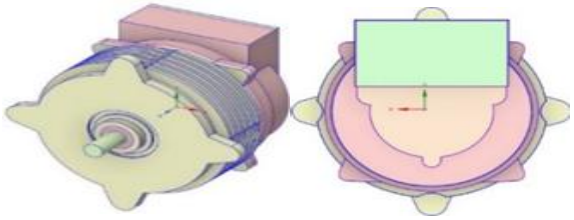

Fig. 4: Geometric Layout of Motor

The 3D motor model which is shown in Fig. 4 is pre-processed in commercial software ANSYS platform and solved in ANSYS Fluent. The mesh generation of the model contains 83, 70,381 cells and 364, 18,111 nodes. The mesh's average quality is 0.867. This study section allows for the determination of the temperature across various components as well as the verification of the temperature calculation results from the earlier LP model.

E Boundary conditions and solver setup

- A pressure inlet at the enclosure entrance is one of the enclosure's boundary conditions. This is used to designate a free intake.

-The enclosure exit has a pressure outlet. This is also helpful in defining a general pressure that leaves the boundary.

-Air domain inside the motor is set to frame motion

- The air gap between the rotor and stator is assigned the same rotational speed as the rotor.

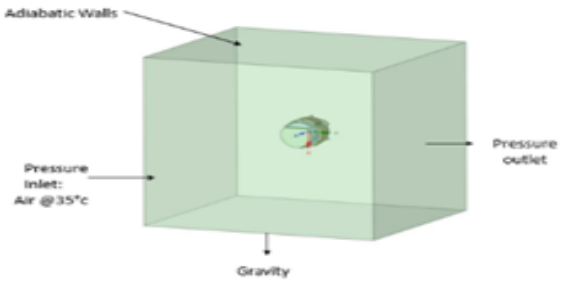

Fig. 5: Applied Boundary Conditions for Thermal Analysis

The SST k-ω model is used in the solver configuration and simulation is performed under steady state conditions. Additionally, the heat source values in Table 6 are given as source terms at their respective regions. Also, the value of material properties assigned to different components of the motor are shown in Table 5.

Table 5: Material Properties of Motor Components

Components	Material Description
Casing	ADC12
Shaft	16MnCr5
Bearing	304 Stainless Steel
Winding	Copper
Magnet	NdFeB N45SH
Stator & Rotor Core	35C270

Table 6: Heat Loss Distribution in Motor Components

Heat Source	Heat loss (W)
Copper Loss	140
Core Loss	43
Magnet Loss	11
Friction Loss	11

FE Experimental setup

An experimental phase was conducted to verify and assess the performance of the developed LH thermal model for PMSM, as well as to ascertain the accuracy of temperature predictions in critical regions of the motor. Below is a summary of the experimental procedures carried out to validate the model. A data acquisition system was used in the testing setup (shown in Fig. 6) to monitor several parameters, including the power factor of each phase, temperature, voltage, current, and injected power. Three RTD sensors were installed in the PMSM for the thermal test. Each RTD was inserted into the end winding section of every phase.

Fig. 6: Experimental Setup for Thermal Testing

G Machine Learning models

Data Description

The dataset comprises 1000 samples, encompassing 41 input variables and 5 output variables derived from the lumped model. The input variables include 35 thermal resistances from the lumped model, ambient temperature, and 5 heat losses. Output variables consist of the temperatures of various components: winding, casing, stator, rotor, and magnet. Before applying machine learning techniques, the dataset underwent preprocessing steps to handle missing values, normalize features, perform feature scaling, and address outliers. Furthermore, feature engineering techniques were utilized to extract pertinent information and augment the predictive capacity of the models.

Selection of Models

To effectively address the multidimensional nature of the dataset and optimize motor performance, a range of machine learning algorithms were explored, including:

i. Linear Regression: It is a parametric approach that models the relationship between the target temperature Y and a set of input features X using a linear equation. The model estimates coefficients that minimize the sum of squared differences between observed and predicted temperatures. Despite its simplicity, linear regression can provide baseline predictions for temperature profiles, particularly useful when the relationships between input features and temperature are approximately linear.

ii. Decision Tree Regression: Non-parametric technique that splits the dataset into subsets based on feature values, constructing a tree where each node represents a decision rule. The tree is built by recursively partitioning the data to minimize variance within each subset. Decision trees can model non-linear relationships and interactions between features.

Random Forest Regression: Random Forest Regression builds an ensemble of decision trees and aggregates their predictions. Each tree is trained on a random subset of the data with feature sampling to ensure diversity and robustness. random forests enhance the predictive accuracy and generalization ability, effectively handling complex interactions and non-linearities in the data.

iii. Support Vector Regression (SVR): Aims to find a function that deviates from the target values within a specified tolerance while minimizing model complexity. Chosen for its effectiveness in managing datasets with complex relationships and possible nonlinearities.

Training and testing of model

To train and evaluate the models' performance, the dataset was divided into the ratio of 3:1 training and testing sets. Cross-validation approaches were used to increase robustness and reduce overfitting. The performance of each model was assessed using appropriate metrics, including R-squared (R^2), Root Mean Squared Error (RMSE), and Mean Absolute Error (MAE). Hyperparameter tuning was used to improve the performance of each machine-learning method. Grid search and randomized search algorithms were used to quickly explore the hyperparameter space and determine the best configuration for each model. In a grid search, a systematic approach is used to explore a predefined set of hyperparameter values. The model is trained and evaluated for each combination of these hyperparameters using cross-validation. The combination that results in the best performance is then selected. For example, hyperparameters such as

the number of trees (n_estimators), maximum depth (max_depth), and maximum features (max_features) are varied across predefined ranges. Randomized Search samples a fixed number of hyperparameter combinations from specified distributions, evaluating the model performance for each combination. It is more efficient than Grid Search, particularly with large hyperparameter spaces. For example, in an SVR model, hyperparameters like the regularization parameter (C), epsilon (epsilon), and kernel parameters (gamma, degree) are sampled from specified distributions.

III. RESULTS AND DISCUSSION

A Results obtained with Lumper Parameter model

The temperature distribution is determined by solving the resistance network depicted in Fig. 2 using MATLAB node equations, with the results presented in Fig. 7. The motor's power loss and the materials employed are listed in Tables 5 and 6 respectively.

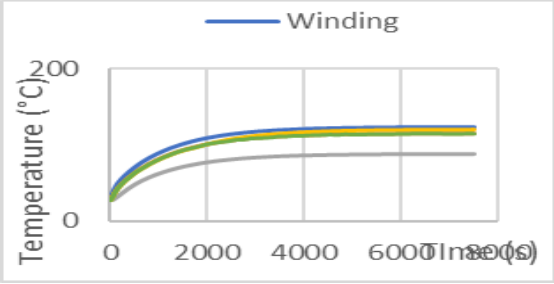

Fig. 7: Temperature Distribution Across Motor Components

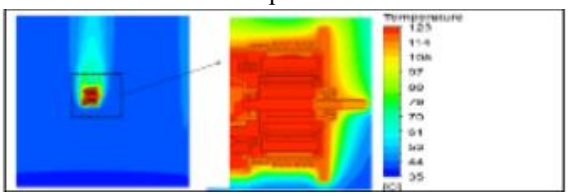

Fig. 8: Temperature Contour of the Entire Motor

From the above graph, it can be seen that the temperature of the winding is the highest, and based on this temperature other component temperatures are determined. This is true since the heat loss in the winding is the highest compared to the other components.

B Results obtained with CFD

The temperature contours of different parts of the motor are shown in Fig. 8-9. Since most of the heat loss is observed in the winding it is expected that the winding will have a high temperature compared to other components of the motor and the same is reflected in CFD simulation. It can also be seen that the air gap between the rotor and stator has a significant influence on the temperature variation in the rotor.

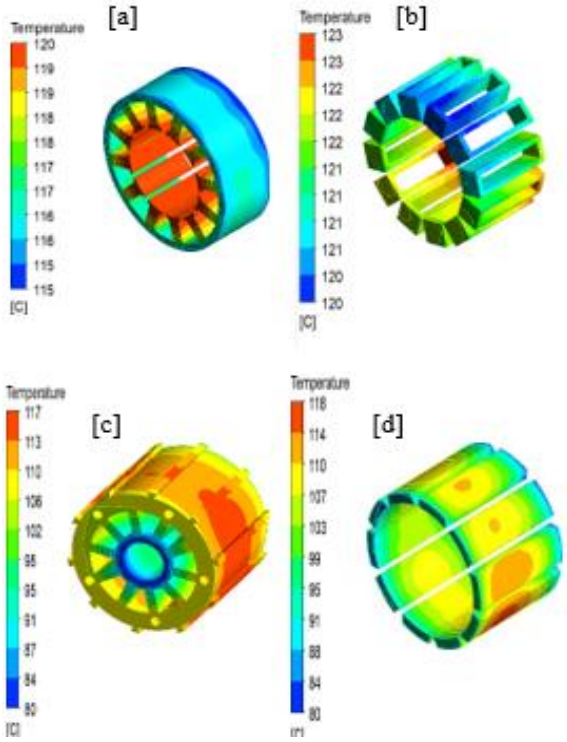

Fig. 9: Temperature Contour Maps for Individual Motor Components: a) Stator b) Winding c) Rotor d) Magnets

From the above simulation, the average temperature of different components at steady state can be determined, and it is compared with values obtained from the lumped model in Table 8.It can be seen that there is a good agreement with the lumped model and CFD results.

Table 8: Comparison of Temperature Predictions from CFD and Lumped Parameter Model

Components	Average Temperature (°C)	LP model Temperature (°C)	Error (%)
Winding	122	123.76	-1.44
Stator	118	120.91	-2.47
Magnet	113	114.87	-1.65
Rotor	113	114.87	-1.65
Casing	86	87.49	-1.73

C Validation with Experimental Results

The experiment was designed to evaluate the accuracy of a lumped thermal model by comparing its predictions to real-world temperature measurements. Conducted over three separate trials, the experiment aimed to test how well the lumped model, which simplifies thermal management analysis by assuming uniform heat distribution, matched actual motor temperatures.

In each trial, temperatures were recorded at various locations on the Permanent Magnet Synchronous Motor (PMSM) using RTD. The average temperatures from these trials were then compared to the temperatures predicted by the lumped thermal model. Fig. 10 illustrates this comparison, showing that the model's predictions for the end-winding temperature deviated by only 1.77% from the experimental measurements.

The small discrepancy between the analytical predictions and the experimental data highlights both the strengths and limitations of the lumped model. While the model's assumption of uniform heat distribution and the use of mean temperature parameters provide a useful approximation, they do not fully capture the complexities observed in the experimental results. In practice, the experimental approach, which involves detailed measurements at specific locations, reveals variations in temperature that the lumped model's assumptions might overlook. These findings underscore the importance of validating theoretical models with experimental data to account for real-world complexities. The lumped model offers a simplified method for thermal analysis, but the experimental data demonstrates that detailed, localized measurements are crucial for a comprehensive understanding of temperature distributions and thermal behavior in electric motors.

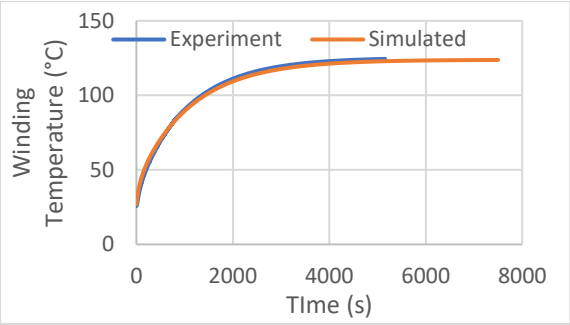

Fig. 10: Temperature Variation in Motor Winding

D Prediction of temperatures using Machine Learning

The performance of different models was determined using performance metrics like R-squared (R^2), Root Mean Squared Error (RMSE), and Mean Absolute Error. The model with high R-squared (R^2), low Root Mean Squared Error (RMSE), and Mean Absolute Error are employed for temperature prediction. From the results, it is evident the linear regression model is the most suitable and can be used to determine the temperature of various components in motor geometry.

The values of different performance metrics are shown in Table 9 for different components of the motor. Further, the linear regression plot of different motor components is shown in Fig. 11. It can be seen the test and the train data in the linear regression model are in good agreement with each other.

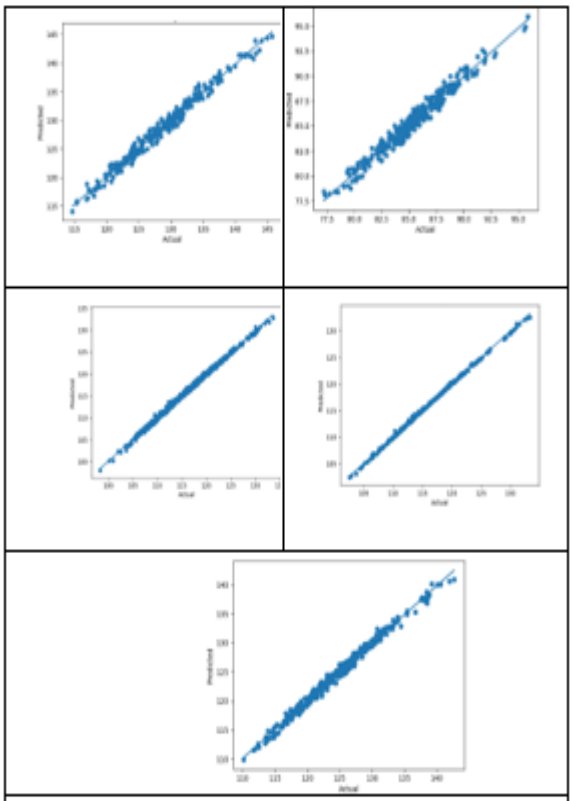

Fig. 11: Linear Regression Analysis of Temperature Prediction for a) Winding temperature b) Casing temperature c) Rotor temperature d) Magnet temperature and e) stator temperature

Table 9: Performance Metrics of Machine Learning Models for Temperature Estimation

Regression Model	R^2	MAE	RMSE
Linear Regression	0.997	0.282	0.352
Decision Tree	0.651	1.529	1.917
Random forest	0.844	1.005	1.279
SVR Regression	0.917	0.773	0.939

Regression Model	R^2	MAE	RMSE
Linear Regression	0.967	0.492	0.588
Decision Tree	0.624	1.581	1.988
Random forest	0.845	1.004	1.276
SVR Regression	0.922	0.738	0.908

Regression Model	R^2	MAE	RMSE
Linear Regression	0.983	0.669	0.831
Decision Tree	0.623	3.104	3.861
Random forest	0.810	2.146	2.734
SVR Regression	0.958	1.018	1.295

Regression Model	R^2	MAE	RMSE
Linear Regression	0.999	0.147	0.207
Decision Tree	0.645	1.555	1.934
Random forest	0.843	1.011	1.284
SVR Regression	0.920	0.743	0.917

Regression Model	R^2	MAE	RMSE
Linear Regression	0.991	0.509	0.661
Decision Tree	0.592	3.150	3.950
Random forest	0.835	1.968	2.518
SVR Regression	0.976	0.742	0.947

IV. CONCLUSION

In the present work, a lumped analysis approach is followed to construct a thermal network to determine the temperature profiles within a PMSM. The approach exhibited rapid and accurate results in the motor's thermal analysis. The steady-state temperatures of various motor components identified through network analysis are noted to be in good agreement with those obtained using CFD.

The LP approach is specifically utilized to estimate the average temperature of individual motor components, considering the complex heat transfer mechanisms and motor design. CFD analysis is employed to assess temperature variations within a motor component. The approach can be adapted for applications with diverse cooling methods, including rotor air cooling, liquid cooling, and internal fans, among others.

Additionally, the proposed thermal analysis approach can incorporate various motor geometries, air gap lengths, and magnet arrangements that can be included in the suggested thermal analysis approach, LH analysis has inherent limits along with its benefits. A promising method that strikes a balance between accuracy and speed is to combine restricted CFD with LH analysis.Machine learning models are employed to provide valuable insights into the effects on the temperature of the motor components due to changes in motor geometry. Among the four models tested and trained, it is observed that predictions made through the Linear regression model yielded results in line with the LP model with the highest R^2 value for temperatures of Winding, Rotor, Casing, Permanent Magnet, and Stator temperatures.

Future research will focus on integrating advanced AI techniques to further enhance thermal analysis. Deep learning models will be explored for their ability to capture complex patterns in temperature data, while reinforcement learning will be applied to optimize cooling strategies and design parameters. This integration aims to address transient real-world conditions, such as varying operational loads and environmental factors, providing more robust and adaptable thermal management solutions. Ultimately, these advancements are expected to lead to more precise, efficient, and adaptable thermal management strategies for modern electric motors, improving performance and reliability in diverse applications.

V. ACKNOWLEDGMENT

The authors are highly thankful to the authorities of NIT Warangal for permitting them to carry out the work at Verroc Tech Centre, Pune. Also, thanks are

due to the cooperation extended by Varroc (Tech center) Elpro compound, Chinchwad Gaon, Chinchwad, Pimpri-Chinchwad, Maharashtra 411033, India.

Conflict of Interest
There are no conflicts of interest.

Declaration of competing interest
The authors declare that they have no known competing financial interests or personal relationships that could have appeared to influence the work reported in this paper. Funding No funding from external agencies is utilized

REFERENCES

[1] Ulbrich, Stefan, Jeanette Kopte, and Jens Proske. "Cooling fin optimization on a TEFC electrical machine housing using a 2-D conjugate heat transfer model." IEEE Transactions on Industrial Electronics 65.2 (2017): 1711-1718.

[2] Valenzuela, M. Anibal, and Juan A. Tapia. "Heat transfer and thermal design of finned frames for TEFC variable-speed motors." IEEE Transactions on Industrial Electronics 55.10 (2008): 3500-3508.

[3] Gronwald, Peer-Ole, and Thorsten A. Kern. "Traction motor cooling systems: A literature review and comparative study." IEEE transactions on transportation electrification 7.4 (2021): 2892-2913.

[4] Gai, Yaohui, et al. "Cooling of automotive traction motors: Schemes, examples, and computation methods." IEEE Transactions on Industrial Electronics 66.3 (2018): 1681-1692.

[5] Rouhani, Hossein, Jawad Faiz, and Caro Lucas. "Lumped thermal model for switched reluctance motor applied to mechanical design optimization." Mathematical and computer modelling 45.5-6 (2007): 625-638.

[6] Pickering, Stephen, et al. "Thermal design of an integrated motor drive." IECON 2006-32nd Annual Conference on IEEE Industrial Electronics. IEEE, 2006.

[7] Boglietti, Aldo, et al. "Impact of different end region cooling arrangements on endwinding heat transfer coefficients in electric motors." 2009 35th Annual Conference of IEEE Industrial Electronics. IEEE, 2009.

[8] Staton, David A., and Andrea Cavagnino. "Convection heat transfer and flow calculations suitable for electric machines thermal models." IEEE transactions on industrial electronics 55.10 (2008): 3509-3516.

[9] Jaeger, Markus, et al. "Thermal analysis of an electrical traction motor with an air-cooled rotor." 2018 IEEE Transportation Electrification Conference and Expo (ITEC). IEEE, 2018.

[10] Chen, Qixu, and Zhongyue Zou. "Lumped-parameter thermal analysis and experimental validation of interior IPMSM for electric vehicle." Journal of Electrical Engineering & Technology 13.6 (2018): 2276-2283.

[11] Wrobel, Rafal. "A technology overview of thermal management of integrated motor drives–Electrical Machines." Thermal Science and Engineering Progress 29 (2022): 101222.

[12] Raj, Jaya Antony Perinba Selvin, et al. "Thermal management strategies and power ratings of electric vehicle motors." Renewable and Sustainable Energy Reviews 189 (2024): 113874.

[13] Pechanek, Roman, and Lukas Bouzek. "Analyzing of two types water cooling electric motors using computational fluid dynamics." 2012 15th International Power Electronics and Motion Control Conference (EPE/PEMC). IEEE, 2012.

[14] Nategh, Shafigh, et al. "Thermal modeling of directly cooled electric machines using lumped parameter and limited CFD analysis." IEEE Transactions on Energy Conversion 28.4 (2013): 979-990.

[15] Zhao, An, et al. "FEM and CFD thermal modeling of an axial-flux induction machine with experimental validation." Case Studies in Thermal Engineering 53 (2024): 103879.

[16] Sali, NVaKP, and Pooja Kulkarni. "Lumped parameter analysis of SMPM synchronous electric motor used for hybrid electric vehicle traction drive." IOSR J. Mechan. Civil Eng 2014 (2014): 42-47.

[17] Liu, Haotian, et al. "Electromagnetic-thermal co-optimization to minimize case-to-winding temperature rise in permanent magnet machines." Applied Thermal Engineering 238 (2024): 122132.

[18] Moon, S. H., Y. H. Jung, and K. W. Kim. "Numerical investigation on thermal-flow characteristics of a totally enclosed fan cooled induction motor." 2016 XXII International Conference on Electrical Machines (ICEM). IEEE, 2016.

[19] Nakahama, Takafumi, et al. "Effects of fan blade forward-swept and inclined amounts in electric motors." IEEE Transactions on Energy Conversion 25.2 (2010): 457-464.

[20] Staton, Dave, Aldo Boglietti, and Andrea Cavagnino. "Solving the more difficult aspects of electric motor thermal analysis." IEEE International Electric Machines and Drives Conference, 2003. IEMDC'03.. Vol. 2. IEEE, 2003.

[21] Amedeo Frilli, Enrico Meli, Daniele Nocciolini, Luca Pugi, Andrea Rindi Energetic optimization of regenerative braking for high speed railway systems Energy Conversion and Management, Vol.129, 2016, Pages 200-215.

[22] Arivoli Anbarasu , Truong Quang Dinh , Somnath Sengupta Novel enhancement of energy management in fuel cell hybrid electric vehicle by an advanced dynamic model predictive control Energy Conversion and Management, Vol. 267, 2022, 115883.

[23] Bin Xu, Ziba Arjmandzadeh,Parametric study on thermal management system for the range of full (Tesla Model S)/ compact-size (Tesla Model 3) electric vehicles Energy Conversion and Management, Vol. 278, 2023, 116753.

[24] Jong Seung Na, Choong-Mo Ryu, Seung Jae Moon,Thermal analysis methods for wound rotor synchronous motors with water-cooling jackets Thermal Science and Engineering Progress,Vol. 46, 2023, 102177.

[25] Jan Zachariae , Matthias Tiesler , Randeep Singh , TimAndy Benning , Christian Schweikert,Silicon carbide based traction inverter cooling in electric vehicle using heat pipesThermal Science and Engineering Progress,Vol. 46, 2023, 102155.

[26] Rafal Wrobel A technology overview of thermal management of integrated motor drives – Electrical Machines Thermal Science and Engineering Progress, Vol. 29, 2022, 101222.

[27] Kral, Christian, et al. "Rotor temperature estimation of squirrel-cage induction motors by means of a combined scheme of parameter estimation and a thermal equivalent model." IEEE Transactions on Industry Applications 40.4 (2004): 1049-1057.

[28] Okoro, Ogbonnaya I. "Steady and transient states thermal analysis of a 7.5-kW squirrel-cage induction machine at rated-load operation." IEEE Transactions on Energy Conversion 20.4 (2005): 730-736.

[29] Kral, Christian, et al. "Comparison of a CFD analysis and a thermal equivalent circuit model of a TEFC induction machine with measurements." IEEE Transactions on Energy Conversion 24.4 (2009): 809-818.

[30] Zine, Wided, et al. "Interests and limits of machine learning-based neural networks for rotor position estimation in EV traction drives." IEEE Transactions on Industrial Informatics 14.5 (2017): 1942-1951.

[31] Dhulipati, Himavarsha, et al. "Advanced design optimization technique for torque profile improvement in six-phase PMSM using supervised machine learning for direct-drive EV." IEEE Transactions on Energy Conversion 34.4 (2019): 2041-2051.

[32] Mukherjee, Debottam, et al. "Application of machine learning for speed and torque prediction of pms motor in electric vehicles." 2020 IEEE 1st International Conference for Convergence in Engineering (ICCE). IEEE, 2020.